IEEE Access
Multidisciplinary | Rapid Review | Open Access Journal

Received July 10, 2019, accepted August 3, 2019, date of publication August 8, 2019, date of current version August 22, 2019.

Digital Object Identifier 10.1109/ACCESS.2019.2933997

Real-Time and Long-Distance Measurement of Displacement Based on Optoelectronic Oscillator

ZHIQIANG FAN, QI QIU, JUN SU, TIANHANG ZHANG, YUE LIN, AND DI JIANG
School of Optoelectronic Science and Engineering, University of Electronic Science and Technology of China, Chengdu 610054, China

Corresponding author: Qi Qiu (qqiu@uestc.edu.cn)

This work was supported in part by the National Natural Science Foundation of China under Grant 61271030, in part by the Fundamental Research Funds for the Central Universities under Grant ZYGX2015J050, and in part by the China Scholarship Council (CSC) Program under Grant 201806070053.

ABSTRACT A frequency-encoded real-time and long-distance displacement measurement method based on two cross-referencing optoelectronic oscillators (OEOs) is proposed and experimentally demonstrated. In the system, one OEO is used for reference, and the other is used for measurement. The initial distance is evaluated by the oscillation frequency and free spectral range of the OEO for reference. The small displacement is calculated by using the frequency of the intermediate frequency (IF) signal generated by mixing the two OEOs. The two OEOs with the same characters are placed in the same environment. This protects the displacement measurement from the influence of the variation of ambient temperature. A high measurement sensitivity, which improves the precision of the displacement measurement, is also implemented due to the accumulative magnification effect at high-order resonant frequency modes. In addition, the low frequency of the IF signal, which is far smaller than the oscillation frequency of the two OEOs, allows a cost-effective and real-time measurement by a frequency counter. The proposed displacement measurement method is demonstrated experimentally. When the sampling time is 1 ms, displacement measurement errors less than ± 3.71 and ± 11.14 μm are realized at emulated distances of around 800m and 6 km, respectively. The real-time velocity and acceleration measurements are also implemented owing to the introduction of a time signal in the measurement process.

INDEX TERMS Microwave photonics, optoelectronic and photonic sensors, displacement measurement, velocity measurement, optoelectronic oscillator.

I. INTRODUCTION

Real-time measurements of distance and its related parameters such as displacement, as well as velocity, are of fundamental importance in various applications, for instances, industrial manufacturing, large-scale structures assembling, and satellite geodetic surveying [1]–[3]. Several optical methods have been regarded attractive solutions to measure the distance and its related parameters due to their unique advantages [4], including the techniques of the intensity-based, the triangulation, the confocal, the doppler sensing, the time-of-flight, the interferometric, and the optoelectronic oscillator (OEO) based.

The associate editor coordinating the review of this article and approving it for publication was Weiren Zhu.

In general, different techniques have their own characteristics and, thus, are applied in different scenarios. The intensity-based techniques with the advantages of the simplest structure and lowest price attract a great deal of attention in the commercial systems. In this system, only a light source and a detector are needed [5]. However, it is limited by the variations of the target reflectivity [6] and the tilt of the target [7]. The triangulation techniques, which usually contains a laser source, a camera optical lens, and an array of detectors [8], also have advantages of low price and fast measurement, but its measurement ability is limited by the size of both the laser beam and detection pixel. The confocal techniques including two types of monochromatic [9] and polychromatic [10] are usually used to measure the distance of several millimeters. The doppler sensing techniques based on a continue-wave laser and a heterodyne detector can directly measure

the velocity of the target [11] in the applications of health care and radar. Nevertheless, the distance information cannot be obtained using this kind of technique. The time-of-flight techniques, which can be implemented using a short light pulse [12] or a frequency modulated continuous light wave [13], provide a solution to simultaneous distance and velocity determination. Although its measurement resolution is limited by the time measurement ability of current instruments. The optical interferometric techniques using Mach-Zehnder interferometer configuration [14] and Michelson interferometer configuration [15] can be realized in the time domain, namely, white-light interferometry (WLI), or in the frequency domain, namely, optical coherence tomography (OCT). The WLI approach based on low-coherence light sources and two arms is usually used as a slow distance or a slow displacement sensor [16] for the measurements of the thickness of silicon wafers [17] and distance in machine-made industrial [18]. To improve the measurement speed, the OCT approach is presented. The measurement speeds up to megahertz provides a special advantage to OCT for the applications of medical imaging and biological detection [19]. However, these techniques mentioned above will be challenged to measure a long-distance of several kilometers with a micro-scale displacement in real time.

Recently, OEO, which has been studied for more than ten years [20], [21] and employed to implement high-performance sensors [22]–[24], is regarded as one tempting solution for the measurement of distance and its related parameters [25]–[29]. Thanks to its high spectral purity and low phase noise [30], it is possible to directly measure the frequency with high precision. Furthermore, the interrogation can be implemented at a high speed by using a high-speed digital signal processor [23]. The high sensitivity is also implemented since the accumulative magnification effect at high-order resonant frequency modes. In [25], to improve the measurement accuracy, the variation of the fiber delay is compensated by a vector network analyzer (VNA) in real time during the distance measurement using an OEO. In [26], an incoherent light source, which is an amplified spontaneous emission (ASE), is used into an OEO for measuring the optical length change. Reconfigurable measurement sensitivity is achieved in this OEO based optical length change measurement system by selecting different oscillation modes. In [27], an intra-loop Michelson interferometer is applied into an OEO to improve the measurement precision. In [28], two OEOs with different oscillation frequency are combined together to measure distance and displacement, where one is used as a reference to stabilize the long length, and the other one is for measurement. In [29], we grouped two OEOs with the same oscillation frequency into a cross-referencing structure, thus, the influence of the environment such as temperature is greatly reduced. Further, the distance and displacement are obtained by measuring the intermediate frequency (IF), which is obtained by mixing the oscillation frequency of the two OEOs into a mixer, thus, the difficulty of measuring frequency is greatly reduced. A quasi-distributed measurement can also be realized due to the use of dense wavelength division multiplexing (DWDM). However, real-time measurement of distance and its related parameters such as displacement, velocity, even acceleration has not been demonstrated in the OEO based distance measurement system mentioned above.

This paper is a continuation of our earlier work reported in [24], [29]. Here we demonstrate a real-time measurement of long-distance displacement based on two cross-referencing OEOs. Thanks to the real-time measurement of displacement, its related parameters, velocity, and acceleration, are also measured in real-time. The use of DWDM based cross-referencing structure greatly reduces the influence of the environment. The measurement of low-frequency IF signal reduces the difficulty of frequency measurement, it provides a potential to measure the displacement in real-time with an inexpensive frequency counter. In the experiment, displacement measurement errors less than ± 3.71 and ± 11.14 μm are demonstrated at emulated distances of around 800 m and 6 km, respectively, when the sampling time is chosen to be 1 ms. In addition, real-time velocity and acceleration measurements are also implemented.

II. PRINCIPLE

Figure 1(a) shows the schematic diagram of the proposed real-time and long-distance displacement measurement method based on two cross-referencing OEOs. Two OEOs with the same architecture and the same oscillation frequency are grouped into a cross-referencing structure using DWDM. In the reference OEO, a light from a laser diode (LD0) is introduced into a Mach-Zehnder modulator (MZM2), whose output is passed through a long fiber, and detected with a photodetector (PD2). The long fiber is shared by the two OEOs with DWDM0. The output of PD2 is amplified by an electrical amplifier (EA), filtered by a bandpass filter (BPF), and sent back to MZM2. Before this, the oscillation signal is introduced to the output through an electrical divider (ED). The output oscillation signal is then divided into two paths by ED3, one of which is used to measure the oscillation frequency and free spectral range (FSR) via an electrical spectrum analyzer (ESA), and the other is introduced into a mixer to mix with the oscillation signal of the measurement OEO. The architecture of the measurement OEO is the same as that of the reference OEO. In the measurement OEO, the measurement area is inserted into the long fiber shared by the two OEOs using a pair of DWDMs. The LD used in the reference OEO is replaced by a tunable light source (TLS), which is used to choose the measurement area in sequence by tuning the wavelength of the TLS. Figure 1(b) shows the schematic diagram of the quasi-distributed measurement, where many different measurement areas are inserted by using many pairs of DWDMs with different wavelengths. It should be noted that the two OEOs should have the same loop length at the initial state. And it is easy to be implemented as the long fiber is shared by the two cross-referencing OEOs.

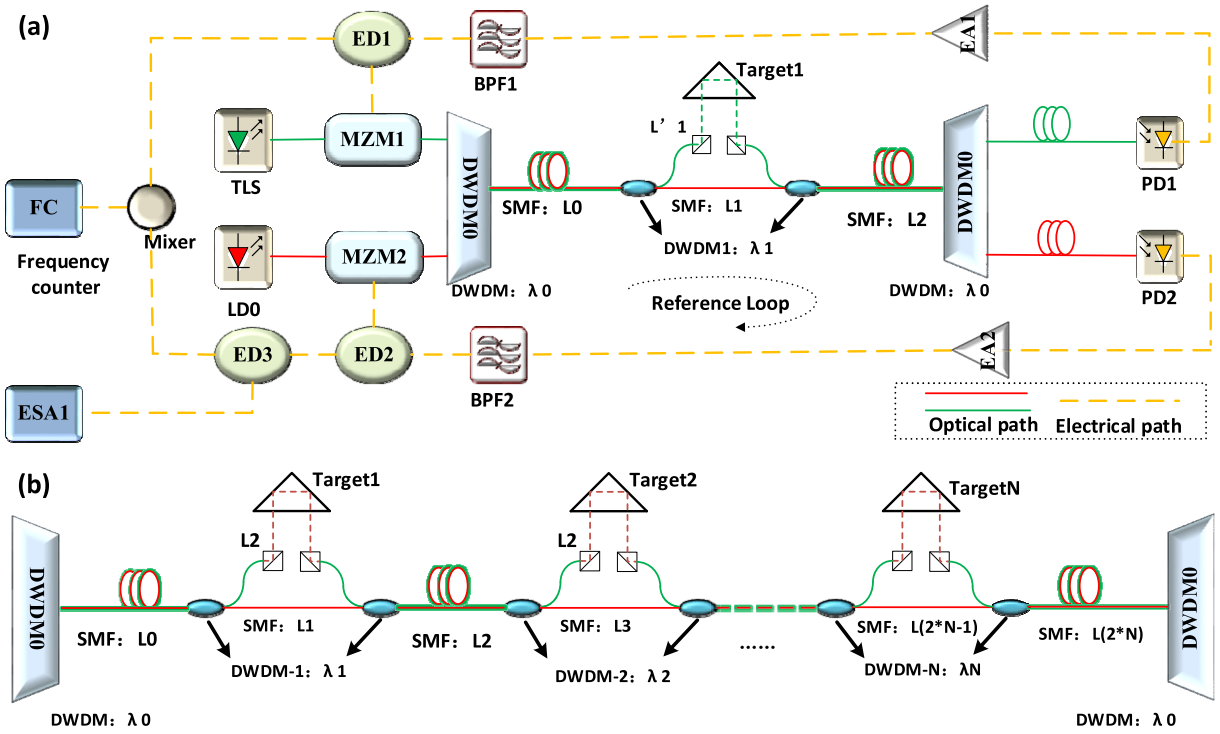

FIGURE 1. The schematic diagram of the proposed real-time and long-distance displacement measurement system. TLS: tunable light source; LD: laser diode; MZM: Mach-Zendher modulator; DWDM: dense wavelength division multiplexing; SMF: single-mode fiber; PD: photoelectric detector; EA: electrical amplifier; BPF: band-pass filter; ED: electrical divider; ESA: electrical spectrum analyzer; FC: frequency counter.

By assuming the initial lengths of the reference OEO and measurement OEO are identical, the initial oscillation frequency of the both OEOs can be written as $f_{ref}^{initial} = k_{ref}/\tau_{initial}$, $f_{mea}^{initial} = k_{mea}/\tau_{initial}$, and the initial oscillation frequency difference between them is $\Delta f_{initial} = (k_{mea} - k_{ref})/\tau_{initial}$, where $f_{ref}^{initial}$ and $f_{mea}^{initial}$ are the initial oscillation frequency of the reference OEO and measurement OEO, respectively, $\tau_{initial}$ is the initial total group delay of the OEO, and k_{ref} and k_{mea} are the values of the high-order oscillation modes of the reference OEO and measurement OEO, respectively. The values of the high-order oscillation modes can be given as the following equations, $k_{ref} = \lfloor f_{ref}^{initial}/f_{FSR}^{initial} \rfloor$, $k_{mea} = \lfloor f_{mea}^{initial}/f_{FSR}^{initial} \rfloor$, where $f_{FSR}^{initial}$ denotes the free spectral range of the reference OEO and measurement OEO, $\lfloor\ \rfloor$ indicates rounding down to the nearest integer.

Thanks to the advantage of the accumulative magnification effect at high-order resonant frequency modes, the measurement precision of the long-distance displacement measurement system can be significantly improved. In an OEO, the high-order frequency can be many times higher than the fundamental frequency, to be more exact, the value of the high-order k can be $10^5 - 10^6$.

The loop lengths of the two OEOs are changed due to the fluctuation of ambient temperature and the movement of the target. Since the two OEOs have an identical initial loop length due to the sharing of the long fiber, the fluctuation of ambient temperature induced loop length changes of the two OEOs are equal. Thus, the oscillation frequencies of the two OEOs and their frequency difference can be rewritten as

$$f_{ref} = k_{ref}/(\tau_{initial} + \Delta\tau_{ref}) \tag{1}$$

$$f_{mea} = k_{mea}/(\tau_{initial} + \Delta\tau_{mea}) \tag{2}$$

$$\Delta f_{target} = k_{mea}/(\tau_{initial} + \Delta\tau_{mea}) - k_{ref}/(\tau_{initial} + \Delta\tau_{ref}) \tag{3}$$

$$\Delta\tau_{ref} = \Delta\tau_{mea} - \Delta\tau_{target} \tag{4}$$

where $\Delta\tau_{ref}$ and $\Delta\tau_{mea}$ are the time delay variations of oscillation loops in the reference OEO and measurement OEO, respectively, and $\Delta\tau_{target}$ is the target movement caused time delay variation in the measurement OEO. When the effect of strain on the shared optical fiber is ignored and only the effect of temperature on the shared optical fiber is considered, the time delay variations of the oscillation loop in the reference OEO can be given as [31],

$$\Delta\tau_{ref} = KL_{ref}^{initial}\Delta T \tag{5}$$

where K is the thermal coefficient of fiber-optical delay which was measured as 39.2 ps/(km·°C) in a standard SMF-28 type single-mode fiber [31], $L_{ref}^{initial}$ is the initial loop length of the reference OEO, ΔT is the temperature variation.

Since $f_{FSR} = 1/(\tau_{initial} + \Delta\tau_{ref})$, the relationship between the target movement induced time delay variation of the measurement OEO and the time delay of the reference OEO can be given as

$$\Delta\tau_{t\arg et} = \frac{\Delta f_{t\arg et} - (k_{ref} - k_{mea}) f_{FSR}}{f_{ref} - \Delta f_{t\arg et}} \cdot (\tau_{initial} + \Delta\tau_{ref}) \tag{6}$$

The loop delays of the reference OEO and measurement OEO are given as $\tau_{ref} = nL_{ref}/c$ and $\tau_{mea} = n(L_{ref} + \Delta L_{target})/c$, respectively, where n is the effective refractive index, c is the velocity of light in a vacuum. Then, the loop length of the reference OEO and the loop length change caused by the movement of the target in the measurement OEO can be expressed as

$$L_{ref} = \frac{c}{nf_{FSR}} \tag{7}$$

$$\frac{\Delta L_{t\arg et}}{L_{ref}} = \frac{\Delta\tau_{t\arg et}}{\tau_{initial} + \Delta\tau_{ref}} = \frac{\Delta f_{t\arg et} - (k_{ref} - k_{mea}) f_{FSR}}{f_{ref} - \Delta f_{t\arg et}} \tag{8}$$

In practice, the measurement speed of the spectral response of the signal generated by the reference OEO, which is measured by using an electrical spectrum analyzer, is too slow to keep with the measurement speed of the target movement caused time delay variation in the measurement OEO, which is measured by using a frequency counter. Thus, the lag in measuring the spectrum of the signal and the measurement error of the frequency of the IF signal will bring errors to the measured displacement.

$$\Delta\tau^m_{t\arg et} = \frac{\Delta f^m_{t\arg et} - (k_{ref} - k_{mea}) f^{initial}_{FSR}}{f^{initial}_{ref} - \Delta f^m_{t\arg et}} \cdot \tau_{initial} \tag{9}$$

$$\Delta f^m_{t\arg et} = \Delta f_{t\arg et} + \Delta f^{error}_{t\arg et} \tag{10}$$

$$L^m_{ref} = \frac{c}{nf^{initial}_{FSR}} \tag{11}$$

$$f^{initial}_{FSR} = 1/\tau_{initial} \tag{12}$$

$$\frac{\Delta L^m_{t\arg et}}{L^m_{ref}} = \frac{\Delta\tau^m_{t\arg et}}{\tau_{initial}} = \frac{\Delta f^m_{t\arg et} - (k_{ref} - k_{mea}) f^{initial}_{FSR}}{f^{initial}_{ref} - \Delta f^m_{t\arg et}} \tag{13}$$

where $\Delta\tau^m_{target}$ is the measured target movement caused time delay variation in the measurement OEO, Δf^m_{target} is the measured frequency of the IF signal, corresponding to the measured frequency difference between the oscillation frequencies of the two OEOs, $f^{initial}_{FSR}$ is the initial free spectral range of the reference OEO, $f^{initial}_{ref}$ is the initial oscillation frequency of the reference OEO, $\Delta f^{error}_{target}$ is the measurement error of the frequency of the IF signal, ΔL^m_{arget} is the measured loop length change caused by the movement of the target in the measurement OEO, L^m_{ref} is the measured loop length of the reference OEO. Then, the temperature variation and measurement error of IF frequency induced measurement error of the target displacement can be written as

$$\begin{aligned}\Delta L^{error}_{t\arg et} &= \Delta L^m_{t\arg et} - \Delta L_{t\arg et} \\ &= \begin{pmatrix} \dfrac{\Delta f^m_{t\arg et} - (k_{ref} - k_{mea}) f^{initial}_{FSR}}{f^{initial}_{ref} - \Delta f^m_{t\arg et}} \cdot L^m_{ref} \\ -\dfrac{\Delta f_{t\arg et} - (k_{ref} - k_{mea}) f_{FSR}}{f_{ref} - \Delta f_{t\arg et}} \cdot L_{ref} \end{pmatrix}\end{aligned} \tag{14}$$

When the loop lengths and the oscillation frequencies of the two OEOs are exactly equal, Eq. (14) can be rewritten as

$$\begin{aligned}\Delta L^{error}_{t\arg et} &= \Delta L^{error,T}_{t\arg et} + \Delta L^{error,M}_{t\arg et} \\ &= \frac{\Delta f^m_{t\arg et}}{f^{initial}_{ref} - \Delta f^m_{t\arg et}} \cdot L^m_{ref} - \frac{\Delta f_{t\arg et}}{f_{ref} - \Delta f_{t\arg et}} \cdot L_{ref}\end{aligned} \tag{15}$$

$$\Delta L^{error,T}_{t\arg et} = \frac{\Delta f_{t\arg et}}{f^{initial}_{ref} - \Delta f^m_{t\arg et}} \cdot L^m_{ref} - \frac{\Delta f_{t\arg et}}{f_{ref} - \Delta f_{t\arg et}} \cdot L_{ref} \tag{16}$$

$$\Delta L^{error,M}_{t\arg et} = \frac{\Delta f^{error}_{t\arg et}}{f^{initial}_{ref} - \Delta f^m_{t\arg et}} \cdot L^m_{ref} \tag{17}$$

where $\Delta L^{error,T}_{target}$ and $\Delta L^{error,M}_{target}$ are the measurement errors of the target displacement induced by the temperature variation and the measurement error of IF frequency, respectively. The measurement error of the target displacement induced by the temperature is the system measuring error. The measurement error of the target displacement induced by the measurement error of IF frequency is the random measuring error, which obeys the normal distribution.

Thanks to the real-time measurement of the target displacement, its related parameters such as velocity and acceleration can also be measured by recording the sampling time when measuring the target displacement. The target velocity and acceleration at different times can be written as

$$v^m_{t\arg et}(t) = \frac{d\Delta L^m_{t\arg et}}{dt} \tag{18}$$

$$a^m_{t\arg et}(t) = \frac{d^2\Delta L^m_{t\arg et}}{dt^2} \tag{19}$$

In practical operations, the measurement of the target displacement is discrete. When the measurement time interval is Δt, the target velocity and acceleration at different times can be rewritten as

$$v^m_{t\arg et}(t) = \frac{\Delta L^m_{t\arg et}(t + \Delta t) - \Delta L^m_{t\arg et}(t - \Delta t)}{2\Delta t} \tag{20}$$

$$a^m_{t\arg et}(t) = \frac{\Delta L^m_{t\arg et}(t + \Delta t) + \Delta L^m_{t\arg et}(t - \Delta t) - 2\Delta L^m_{t\arg et}(t)}{\Delta t} \tag{21}$$

According to Eqs. (2) to (15), the measurement error of the target displacement in a single-OEO measurement system

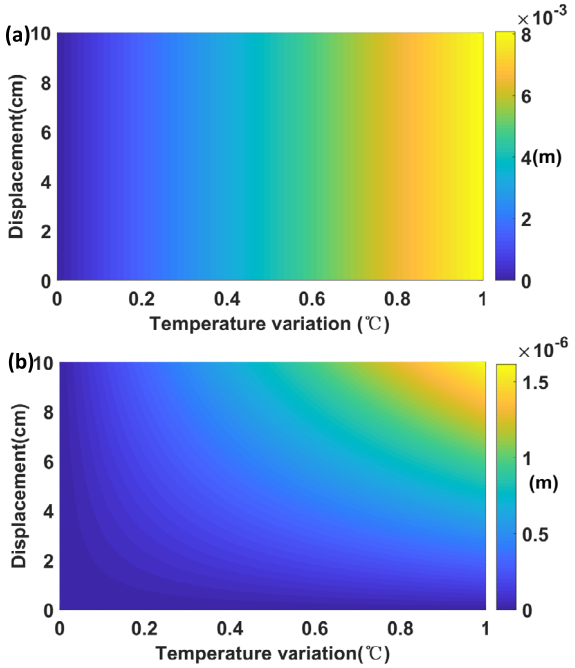

FIGURE 2. The calculated temperature induced measurement errors of the target displacement in (a) a single-OEO measurement system, and (b) the proposed dual-OEO measurement system at different target displacement.

and the proposed dual-OEO measurement system are both affected by the temperature variation. When the oscillation frequency of the OEO is 10 GHz, the thermal coefficient of fiber-optical delay is 39.2 ps/km·°C, and the initial loop length of the OEO is 1 km, the temperature caused measurement errors of the target displacement in a single-OEO measurement system and the proposed dual-OEO measurement system are calculated in Fig. 2.

As shown in Fig. 2 (a), the measurement error of a single-OEO measurement system is up to 8 mm when the temperature changes 1°C. In contrast, as shown in Fig. 2(b), the measurement error of the proposed dual-OEO measurement system is as low as 1.6 μm when the temperature changes 1°C and the target displacement is 10 cm. Clearly, the temperature variation induced measurement error of the target displacement in the proposed dual-OEO measurement system is significantly reduced than that in a single-OEO measurement system.

III. EXPERIMENTAL RESULTS AND DISCUSSIONS

A proof-of-concept experiment is carried out based on the setup in Fig. 1(a). Two laser sources with wavelengths of 1550.12 nm and 1550.92 nm, respectively, are applied as the LD and TLS, respectively, and both the output light waves from the two laser sources have (Yenista optics TLS-AG) a power of 10 dBm. The two MZMs are two single-drive intensity LiNbO3 modulators (OCLARO F-10) with a 3-dB bandwidth of 11 GHz and insertion loss of 6 dB. The two PDs (Kang Guan KG-PD-10G) have a same responsivity of 0.8 A/W and 3-dB bandwidth of 11GHz. The two EAs have

TABLE 1. Simulated velocities of the target in different time periods.

Time periods(ms)	speeds of change in time delay (ps/s)	simulated velocities of the target (μm/ms)
0-530	7	2.099
530-770	18	5.396
770-2000	37	11.092
2000-2550	44	13.191
2550-2780	54.5	16.339
2780-8620	74	22.185
8620-9560	37	11.092
9560-10180	29	8.694
10180-10410	19	5.696
10410-17120	0	0
17120-18290	-37	-11.092
18290-18680	-7	-2.099
18680-18910	-17.5	-5.246
18910-33210	-37	-11.092
33210-33530	0	0

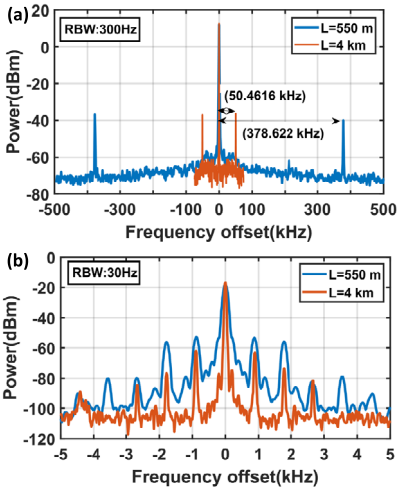

FIGURE 3. The measured electrical spectrums of (a) the generated signals of the reference OEO and (b) the intermediate frequency (IF) signal when the loop length of the reference OEO is around 4 km or 550 m.

a same response of 40GHz. The two BPFs have a same center frequency of 10.6GHz and same 3-dB bandwidth of 13MHz. The electrical spectrums of the oscillation signal from the reference OEO and the intermediate frequency (IF) signal from the electrical mixer are measured by using an electrical spectrum analyzer (Anritsu MS2725C). The frequency of the IF signal is measured by using a frequency counter (Agilent 53230A). The target displacement and its related parameter velocity are simulated by using a programmable and tunable optical fiber delay line with a resolution of 39.6 fs. Assuming the target starts moving at zero, the programmed speeds of change in time delay and the corresponding simulated velocities of the target in different time periods are shown in Table 1.

To evaluate the measuring ability of the proposed displacement measurement system at different distances, two systems with loop lengths of about 4 km and 550 m are designed. Figure 3 shows the measured spectrums of the generated signals of the reference OEO and the IF signal when the

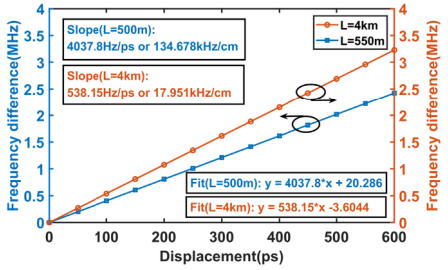

FIGURE 4. Measured relationship between frequency difference and different length change when the loop length of the reference OEO is about 4 km or 550 m.

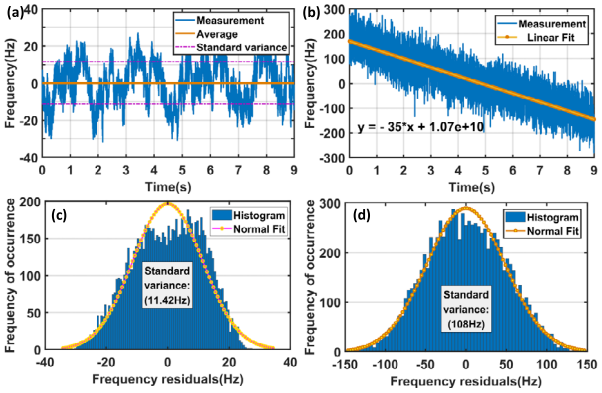

FIGURE 5. The measured frequencies of (a) the IF signal in the proposed dual-OEO displacement measurement system and (b) the oscillation signal in a single-OEO displacement measurement system when the length of the fiber used in the systems is about 4 km. (c) The histogram of the measured data in (a). (d) The histogram of the fitting residual of the oscillation frequency in (b).

loop length of the reference OEO is 4 km or 550m, approximately. When the loop length of the reference OEO is about 4 km, the initial oscillation frequency of the reference OEO is measured as 10664330499 Hz, and the initial fundamental frequency, namely the initial free spectral range $f_{FSR}^{initial}$, is measured to be 50462 Hz. Then, the value of the high-order oscillation modes can be calculated as $k_{ref} = \lfloor 10664330499/50462 \rfloor = 211333$. According to Eq. (11), the simulated length of the fiber and the simulated distance in a vacuum are 4078.645296 m and 5940.954738 m, respectively, when $c = 299792458$ m/s and $n = 1.4566$. When the loop length of the reference OEO is about 550 m, the initial oscillation frequency of the reference OEO and the initial fundamental frequency are measured to be 10664476363 Hz and 378622 Hz, respectively. Then, the value of the high-order oscillation modes can be calculated as $k_{ref} = \lfloor 10664476363/378622 \rfloor = 28166$. The simulated length of the fiber and the simulated distance in a vacuum are 543.593872 m and 791.798834 m, respectively. The spectrums of the IF signals are measured in Fig. 3(b) when the measurement system has different loop lengths of around 4 km and 550 m, respectively. Clearly, the phase noise of the IF signal in the system with a loop length of about 4 km is lower than that in the system with a loop length of about 550 m, due to the longer loop length in the OEO reduces the phase noise of the oscillation signal. The lower phase noise of the IF signal makes its frequency measurement more accurate. Figure 4 shows the measured relationship between the frequency of the IF signal and the displacement of the target, the sensitivities of the systems with emulated distances of around 6 km and 800 m are measured to be 17.951 and 134.687 kHz/cm, respectively.

The influence of the temperature variation on the measurement errors of the proposed dual-OEO displacement measurement system and a single-OEO displacement measurement system is evaluated in Fig. 5. The loop lengths of the dual-OEO or single-OEO are same as around 4 km and the oscillation frequencies of the OEOs are same as about 10.664 GHz. By placing the long fiber in an environment where the temperature is not controlled, keeping the target stationary, and setting the sample rate of the frequency counter to be 1 kHz, the frequency variations of the IF signal in the proposed dual-OEO measurement system and the oscillation signal in a single-OEO measurement system are measured in Figs. 5(a) and 5(b). In the proposed dual-OEO measurement system, the frequency variation of the IF signal is within ±20 Hz corresponding to a measurement error of ±11.14 μm at a measurement distance of about 6 km. The histogram of the measured data, as shown in Fig. 5(c), shows a Gaussian profile having a standard variance of 11.42 Hz. This means that the measurement error of the proposed dual-OEO measurement system is almost free to the temperature variation. In the single-OEO measurement system, the frequency of the oscillation signal goes down 35 Hz per second due to the influence of the temperature variation. It means the temperature variation induces a measurement error of 19.50 μm per second during this measurement. Note that the measurement error dependents the rate of change in temperature. The histogram of the fitting residual of the oscillation frequency is shown in Fig. 5(d). It shows a Gaussian profile with a standard variance of 108 Hz, which is higher than that of the measured data of the IF signal in the proposed dual-OEO measurement system. This means that the measuring of the IF signal using a frequency counter in the proposed dual-OEO measurement system provides an advantage of higher precision than the measuring of the oscillation signal in the single-OEO measurement system.

Figure 6 shows the measured frequency of the IF signal by a frequency counter with different sample rates when the target has a same trajectory. The trajectory of the target is shown in the inset in Fig. 6(a). The length of the optical fiber used in the reference OEO is 550 m, approximately. As shown in Fig. 6(a), the frequency responses of the IF signal are measured at different sample rates of 10 kHz, 1 kHz, 100 Hz, and 10Hz. These measured frequency responses at different rates are consistent. Figure 6(b) shows the measured frequency of the IF signal when the target is stationary in the starting position (Point A, inset of Fig. 6(a)). When the sample rates are 10 kHz, 1 kHz, 100 Hz, and 10Hz, the frequency variations of the IF signals are within ±100 Hz, ±50 Hz, ±25 Hz, and ±15 Hz, corresponding to the measurement

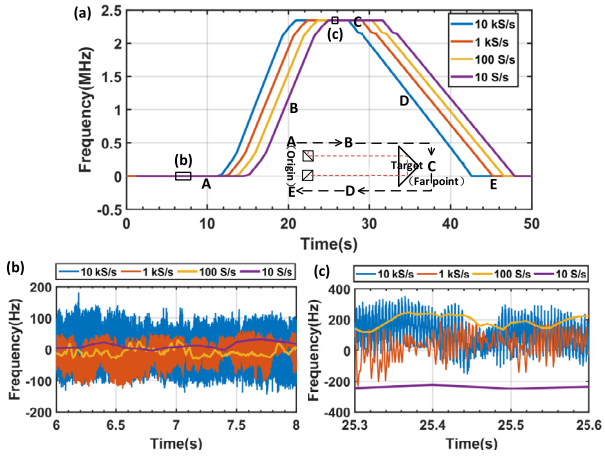

FIGURE 6. (a) The measured frequency of the IF signal by a frequency counter with the different sample rates of 10 kHz, 1 kHz, 100 Hz, and 10Hz, when the length of the fiber used in the systems is about 550 m. (b) The measured frequency of the IF signal during the time range from 6 to 8 s. (c) The measured frequency of the IF signal during the time range from 25.3 to 25.6 s.

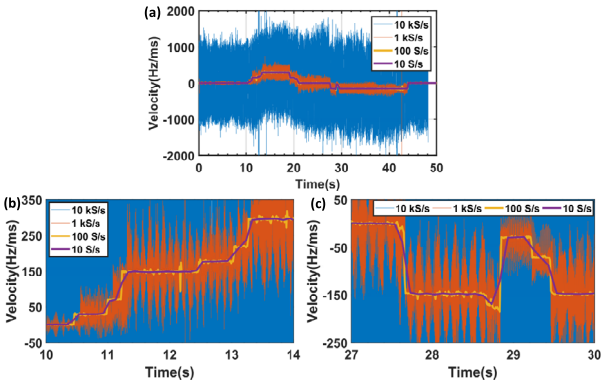

FIGURE 7. (a) The calculated velocity of the frequency change of the IF signal when the sample rates are selected to be 10 kHz, 1 kHz, 100 Hz, and 10Hz, and the length of the fiber used in the systems is about 550 m. (b) The calculated velocity of the frequency change of the IF signal during the time range from 10 to 14 s. (c) The calculated velocity of the frequency change of the IF signal during the time range from 27 to 30 s.

errors of ± 7.42 μm, ± 3.71 μm, ± 1.86 μm, ± 1.11 μm, respectively, at a measurement distance of about 800 m in a vacuum. Clearly, a higher sample rate introduces a higher measurement error. The measurement results provide a reference for the balance between the measurement speed and measurement precision in practical application. Figure 6 (c) shows the measured frequency of the IF signal when the target is stationary in the farthest simulated displacement position (Point C, inset of Fig. 6(a)). A frequency difference of 400 Hz, corresponding to a measured displacement difference of 29.70 μm, is found. That is due to the repeatability of the programmable and tunable optical fiber delay line.

Using the measured frequency of the IF signal in Fig. 6, the velocity of the frequency change is calculated in Fig. 7. Obviously, these calculated velocities of the frequency changes at different rates are consistent. The vibration of the target, that is the mirror in the programmable and tunable optical fiber delay line, caused by its high-speed movement is also

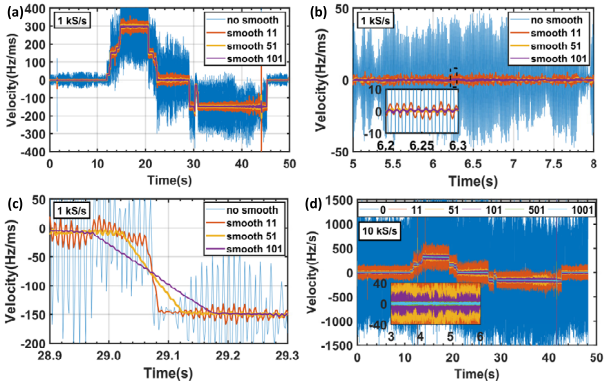

FIGURE 8. (a) The calculated and smoothed velocity of the frequency change of the IF signal when the sample rate is 1 kHz and the length of the fiber used in the systems is about 550 m. (b) The calculated velocity of the frequency change of the IF signal during the time range from 5 to 8 s. (c) The calculated velocity of the frequency change of the IF signal during the time range from 28.9 to 29.3 s. (d) The calculated and smoothed velocity of the frequency change of the IF signal when the sample rate is 10 kHz and the length of the fiber used in the systems is about 550 m.

observed by using a higher sample rate. In the proposed dual-OEO displacement measurement system, a higher sample rate provides a better detail description capability. However, A larger measurement error is found when the sample rate is higher, which can also be found in the measuring results of the target displacement in Fig. 6. One solution is to smooth the measured data through moving average filtering algorithm, which is a lowpass filter with filter coefficients equal to the reciprocal of the span.

Figure 8 shows the calculated and smoothed velocity of the frequency change of the IF signal. The length of the optical fiber used in the reference OEO is around 550 m, corresponding to an emulated distance of around 800 m in a vacuum. As shown in Fig. 8(a), different spans of the moving average of 11, 51, and 101 are chosen to smooth the velocity of the frequency change of the IF signal when the sample rate is 1 kHz. Clearly, the measurement error is effectively reduced by using the moving average filtering algorithm. Figure 8(b) shows the zoom in view of the velocity of the frequency change during the time range from 5 to 8 s, the velocity of the frequency change of the IF signal is within ± 50 Hz/ms, corresponding to the measurement error of ± 3.71 μm/ms. When the spans of the moving average are 11, 51, and 101, the velocities of the frequency change of the IF signal are within ± 4, ± 1, and ± 1 Hz/ms, corresponding to the measurement errors of ± 0.297, ± 0.0742, and ± 0.0742 μm/ms, respectively. It should be noted that the moving average is a lowpass filter with filter coefficients equal to the reciprocal of the span, which inhibits the response of the measurement system to the high-frequency changes of the velocity of the frequency change, especially the step changes. This can be observed in Fig. 8(c). When the sample rate is chosen to be 10 kHz, the different spans of the moving average of 11, 51, 101, 501, and 1001 are chosen to smooth the velocity of the frequency change of the IF signal in Fig. 8(d). The inset shows the zoom in view of the velocity of the frequency change during the

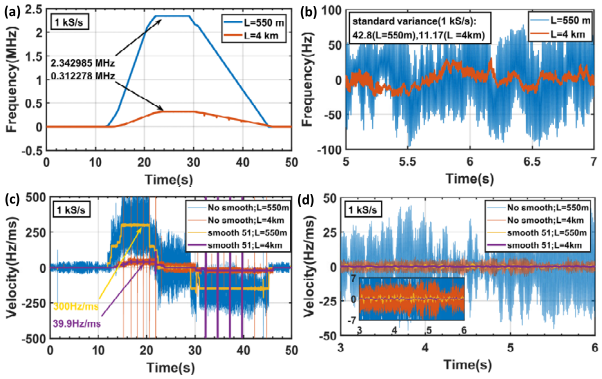

FIGURE 9. (a) The measured frequency of the IF signal by a frequency counter with a sample rate of 1 kHz when the length of the fiber used in the systems is about 550 m or 4 km. (b) The measured frequency of the IF signal during the time range from 5 to 7 s. (c) The calculated and smoothed velocity of the frequency change of the IF signal when the sample rate is 1 kHz and the length of the fiber used in the systems is about 550 m or 4 km. (d) The calculated velocity of the frequency change of the IF signal during the time range from 3 to 6 s.

time range from 3 to 6 s. When the spans of the moving average are 11, 51, 101, 501, and 1001, the velocities of the frequency change of the IF signal are within ±150, ±50, ±25, ±5, and ±3 Hz/ms, corresponding to the measurement errors of ±11.1, ±3.71, ±1.86, ±0.371, and ±0.223 μm/ms, respectively.

The measuring ability of the proposed dual-OEO displacement measurement system with different distances is also evaluated in Fig. 9. A long fiber with a length of around 550 m or 4 km, corresponding to an emulated distance of around 800 m or 6 km in a vacuum, is used in the reference OEO. According to Fig. 9(a), the largest frequency shifts of the systems with different emulated distances of around 800 m and 6 km are measured to be 2.342985 and 0.312287 MHz, corresponding to different displacements of 0.173958 and 0.173966 m, respectively, when the target is stationary in the farthest simulated displacement position (Point C, inset of Fig. 6(a)). The measured results of both the experiment agree well with the real value of 0.173967 m. Figure 9(b) shows the measured frequency of the IF signal when the target is stationary in the starting position (Point A, inset of Fig. 6(a)). The frequency variations of the IF signals are within ±50 and ±20 Hz, corresponding to the measurement errors of ±3.71 and ±11.14 μm, at different emulated distances of around 800 and 6 km, respectively. The velocity of the target is calculated in Figs. 9(c) and (d). When the target is stationary at the starting position, the velocities of the frequency change of the IF signal in the system with different emulated distances of around 800 and 6 km are within ±50 and ±7 Hz/ms, corresponding to the measurement error of ±3.71 and ±3.90 μm/ms, respectively. When the span of the moving average is 51, the velocities of the frequency change of the IF signal are within ±1 and ±0.5 Hz/ms, corresponding to the measurement errors of ±0.0742 and ±0.279 μm/ms, respectively. Assuming the target starts moving at zero, the measured velocities of the target at different time periods and different simulated distances are measured

TABLE 2. Measured velocities of the target at different times and different simulated distances.

Time periods (ms)	Simulated velocities (μm/ms)	Measured velocities (μm/ms)	
		L=550m	L=4km
0-530	2.099	2.153±0.223	2.061±0.279
530-770	5.396	5.346±0.223	5.404±0.223
770-2000	11.092	11.063±0.297	11.030±0.279
2000-2550	13.191	13.216±0.371	13.203±0.446
2550-2780	16.339	16.334±0.297	16.434±0.279
2780-8620	22.185	22.274±0.594	22.228±0.446
8620-9560	11.092	11.063±0.371	10.975±0.335
9560-10180	8.694	8.687±0.371	8.802±0.335
10180-10410	5.696	5.680±0.371	5.794±0.391
10410-17120	0	0±0.519	0±0.558
17120-18290	-11.092	-11.137±0.445	-11.142±0.446
18290-18680	-2.099	-2.190±0.223	-2.061±0.279
18680-18910	-5.246	-5.234±0.223	-5.292±0.223
18910-33210	-11.092	-11.137±0.445	-11.142±0.446
33210-33530	0	0±0.0742	0±0.223

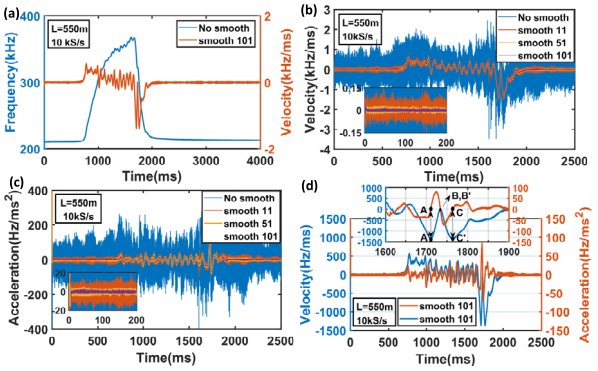

FIGURE 10. (a) The measured frequency of the IF signal by a frequency counter with a sample rate of 1 kHz when the length of the fiber used in the systems is about 550 m. (b) The calculated and smoothed velocity of the frequency change of the IF signal. (c) The calculated and smoothed acceleration of the frequency change of the IF signal. (d) The smoothed velocity and acceleration of the frequency change of the IF signal.

in Table 2, the measuring results agree well with the real values. It can be found that the measurement results fluctuate more when the target has a higher velocity. That is because of the high velocity of the target results in great vibration of the optical delay line.

To further evaluate the real-time measurement capability of the proposed dual-OEO displacement system. The optical fiber delay line is replaced by an equal length of optical fiber. Its random variation, which is caused by the mechanical shock on the fiber, is observed. In this test, the fluctuation of fiber length is used to simulate the movement of the target and the sample rate is chosen to be 10 kHz. Figure 10 shows the measured displacement, the velocity, and the acceleration of the simulated moving target. A random fluctuation lasting for about 1.25 s was recorded in real time, further proving the real-time measurement capability of the system. In this test, the largest displacement, velocity, and acceleration are measured to be 0.027306 m, −102.246 μm/ms, and 5.881 μm/ms^2 respectively.

IV. CONCLUSION

In summary, we proposed and realized a frequency-encoded real-time and long-distance displacement measurement system based on two cross-referencing optoelectronic oscillators (OEOs). In the proposed system, a high measurement sensitivity was implemented due to the accumulative magnification effect at high-order resonant frequency modes. The influence of the variation of ambient temperature on the displacement measurement was greatly reduced as the cross-referencing structure of the two OEOs having an identical geometry, which were placed in the same environment. Real-time and cost-effective measurement was realized using a frequency counter since the low frequency of the IF signal. In the experiments, the measurement of displacement and its related parameters such as velocity were demonstrated. A displacement measurement error less than ± 11.14 μm and a velocity measurement error less than ± 3.90 μm/ms were demonstrated at an emulated distance of around 6 km and a sampling time of 1 ms. A displacement measurement error less than ± 3.71 μm and a velocity measurement error less than ± 3.71 μm/ms were demonstrated at an emulated distance of around 800 m and a sampling time of 1 ms. Based on these advantages above, the proposed displacement measurement system may find important applications in industrial manufacturing, large-scale structures assembling, and satellite geodetic surveying.

REFERENCES

[1] M. E. Pritchard and M. Simons, "A satellite geodetic survey of large-scale deformation of volcanic centres in the central Andes," *Nature*, vol. 418, no. 6894, pp. 167–171, Jul. 2002.
[2] W. T. Estler, K. L. Edmundson, G. N. Peggs, and D. H. Parker, "Large-scale metrology—An update," *CIRP Ann.*, vol. 51, no. 2, pp. 587–609, Jan. 2002.
[3] R. Pierce, J. Leitch, M. Stephens, P. Bender, and R. Nerem, "Intersatellite range monitoring using optical interferometry," *Appl. Opt.*, vol. 47, no. 27, pp. 5007–5019, Sep. 2008.
[4] G. Berkovic and E. Shafir, "Optical methods for distance and displacement measurements," *Adv. Opt. Photon.*, vol. 4, no. 4, pp. 441–471, 2012.
[5] H. Golnabi and P. Azimi, "Design and operation of a double-fiber displacement sensor," *Opt. Commun.*, vol. 281, no. 4, pp. 614–620, Feb. 2008.
[6] P. Li, H. Zhang, Y. Zhao, and L.-Z. Yang, "New compensation method of an optical fiber reflective displacement sensor," *Proc. SPIE*, vol. 3241, pp. 474–477, Nov. 1997.
[7] J. Liu, K. Yamazaki, Y. Zhou, and S. Matsumiya, "A reflective fiber optic sensor for surface roughness in-process measurement," *J. Manuf. Sci. Eng.*, vol. 124, no. 3, pp. 515–522, Jul. 2002.
[8] Z. Ji and M. C. Leu, "Design of optical triangulation devices," *Opt. Laser Technol.*, vol. 21, no. 5, pp. 339–341, Oct. 1989.
[9] L. Yang, G. Wang, J. Wang, and Z. Xu, "Surface profilometry with a fibre optical confocal scanning microscope," *Meas. Sci. Technol.*, vol. 11, no. 12, pp. 1786–1791, Jul. 2000.
[10] J. Garzón, J. Meneses, G. Tribillon, T. Gharbi, and A. Plata, "Chromatic confocal microscopy by means of continuum light generated through a standard single-mode fibre," *J. Opt. A, Pure Appl. Opt.*, vol. 6, no. 6, pp. 544–548, Apr. 2004.
[11] J. W. Foreman, Jr., E. W. George, and R. D. Lewis, "Measurement of localized flow velocities in gases with a laser Doppler flowmeter," *Appl. Phys. Lett.*, vol. 7, no. 4, pp. 77–78, Jun. 1965.
[12] J. Pehkonen, P. Palojarvi, and J. Kostamovaara, "Receiver channel with resonance-based timing detection for a laser range finder," *IEEE Trans. Circuits Syst. I, Reg. Papers*, vol. 53, no. 3, pp. 569–577, Mar. 2006.
[13] E. Shafir and G. Berkovic, "Compact fibre optic probe for simultaneous distance and velocity determination," *Meas. Sci. Technol.*, vol. 12, no. 7, pp. 943–947, Apr. 2001.
[14] A. Dandridge and A. B. Tveten, "Phase compensation in interferometric fiber-optic sensors," *Opt. Lett.*, vol. 7, no. 6, pp. 279–281, Jun. 1982.
[15] B. S. Lee and T. C. Strand, "Profilometry with a coherence scanning microscope," *Appl. Opt.*, vol. 29, no. 26, pp. 3784–3788, Sep. 1990.
[16] Y.-J. Rao and D. A. Jackson, "Recent progress in fibre optic low-coherence interferometry," *Meas. Sci. Technol.*, vol. 7, no. 7, pp. 981–999, Jul. 1996.
[17] W. J. Walecki, A. Pravdivtsev, M. Santos, II, and A. Koo, "High-speed high-accuracy fiber optic low-coherence interferometry for *in situ* grinding and etching process monitoring," *Proc. SPIE*, vol. 6293, Aug. 2006, Art. no. 62930D.
[18] M. L. Dufour, G. Lamouche, S. Vergnole, B. Gauthier, C. Padioleau, M. Hewko, S. Lévesque, and V. Bartulovic, "Surface inspection of hard to reach industrial parts using low-coherence interferometry," *Proc. SPIE*, vol. 6343, Sep. 2006, Art. no. 63431Z.
[19] J. M. Schmitt, "Optical coherence tomography (OCT): A review," *IEEE J. Sel. Topics Quantum Electron.*, vol. 5, no. 4, pp. 1205–1215, Jul. 1999.
[20] X. S. Yao and L. Maleki, "Optoelectronic oscillator for photonic systems," *IEEE J. Quantum Electron.*, vol. 32, no. 7, pp. 1141–1149, Jul. 1996.
[21] Z. Fan, Q. Qiu, J. Su, T. Zhang, and Y. Lin, "Phase noise measurement of an optoelectronic oscillator based on the photonic-delay line cross-correlation method," *Opt. Lett.*, vol. 44, no. 8, pp. 1992–1995, Apr. 2019.
[22] X. Zou, X. Liu, W. Li, P. Li, W. Pan, L. Yan, and L. Shao, "Optoelectronic oscillators (OEOs) to sensing, measurement, and detection," *IEEE J. Quantum Electron.*, vol. 52, no. 1, Jan. 2016, Art. no. 0601116.
[23] J. Yao, "Optoelectronic oscillators for high speed and high resolution optical sensing," *J. Lightw. Technol.*, vol. 35, no. 16, pp. 3489–3497, Aug. 15, 2017.
[24] Z. Fan, J. Su, T. Zhang, N. Yang, and Q. Qiu, "High-precision thermal-insensitive strain sensor based on optoelectronic oscillator," *Opt. Express*, vol. 25, no. 22, pp. 27037–27050, Oct. 2017.
[25] T. Zhang, J. Zhu, T. Guo, J. Wang, and S. Ye, "Improving accuracy of distance measurements based on an optoelectronic oscillator by measuring variation of fiber delay," *Appl. Opt.*, vol. 52, no. 15, pp. 3495–3499, May 2013.
[26] X. Zou, M. Li, W. Pan, B. Luo, L. Yan, and L. Shao, "Optical length change measurement via RF frequency shift analysis of incoherent light source based optoelectronic oscillator," *Opt. Express*, vol. 22, no. 9, pp. 11129–11139, May 2014.
[27] J. Lee, S. Park, D. H. Seo, S. H. Yim, S. Yoon, and D. Cho, "Displacement measurement using an optoelectronic oscillator with an intra-loop Michelson interferometer," *Opt. Express*, vol. 24, no. 19, pp. 21910–21920, Sep. 2016.
[28] J. Wang, J. Yu, W. Miao, B. Sun, S. Jia, W. Wang, and Q. Wu, "Long-range, high-precision absolute distance measurement based on two optoelectronic oscillators," *Opt. Lett.*, vol. 39, no. 15, pp. 4412–4415, Aug. 2014.
[29] Z. Fan, J. Su, T. Zhang, N. Yang, and Q. Qiu, "High-precision and long-range distance measurement independent of temperature based on two optoelectronic oscillators," in *Proc. Int. Top. Meeting Microw. Photon. (MWP)*, Beijing, China, Oct. 2017, pp. 1–4.
[30] Z. Fan, Q. Qiu, J. Su, and T. Zhang, "Tunable low-drift spurious-free optoelectronic oscillator based on injection locking and time delay compensation," *Opt. Lett.*, vol. 44, no. 3, pp. 534–537, Feb. 2019.
[31] N. Yang, J. Su, Z. Fan, and Q. Qiu, "High precision temperature insensitive strain sensor based on fiber-optic delay," *Sensors*, vol. 17, no. 5, p. 1005, May 2017.

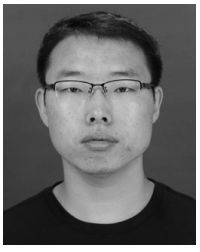

ZHIQIANG FAN received the B.Eng. degree in electronic science and technology (optoelectronic engineering and optical communication) from the University of Electronic Science and Technology of China (UESTC), Chengdu, China, in 2015, where he is currently pursuing the Ph.D. degree with the School of Optoelectronic Science and Engineering.

He is currently a joint Training Student with the Microwave Photonics Research Laboratory, School of Electrical Engineering and Computer Science, University of Ottawa, Ottawa, ON, Canada. His current research interests include photonic generation of microwave waveforms, phase noise measurement, fiber photonic sensors, and integrated microwave photonics.

QI QIU received the B.S. degree in laser from the Huazhong University of Science and Technology, Wuhan, China, in 1985, and the Ph.D. degree in optical engineering from the University of Electronic Science and Technology of China (UESTC), Chengdu, China, in 2007.

He is currently a Professor with UESTC. He has published more than 100 international journals and conferences. His current research interests include optical communication, microwave photonics, and optical fiber sensor.

JUN SU received the B.S. and Ph.D. degrees in electronic science and technology (optoelectronic engineering and optical communication) and optical engineering from the University of Electronic Science and Technology of China (UESTC), Chengdu, China, in 2007 and 2014, respectively.

He is currently an Associate Researcher with UESTC. His current research interests include microwave photonics and optical fiber sensor.

TIANHANG ZHANG received the B.S. degree in automation from the Anhui University of Technology, Maanshan, China, in 2011, and the M.A.Sc. degree in pattern recognition from the University of Electronic Science and Technology of China (UESTC), Chengdu, China, in 2014, where he is currently pursuing the Ph.D. degree with the School of Optoelectronic Science and Engineering.

His current research interests include microwave photonics and optical fiber sensor.

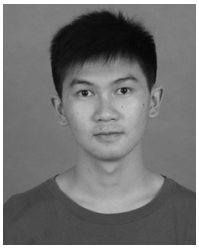

YUE LIN received the B.S. degree in applied physics from the Qingdao University of Technology, Qingdao, China, in 2016. He is currently pursuing the Ph.D. degree with the School of Optoelectronic Science and Engineering, UESTC.

His current research interests include microwave photonics and optical communication.

DI JIANG received the B.S. degree in electronic science and technology (optoelectronic engineering and optical communication) from Zhejiang University (ZJU), Hangzhou, China, in 2016. He is currently pursuing the Ph.D. degree with the School of Optoelectronic Science and Engineering, UESTC.

His current research interests include microwave photonics and optical communication.